Giant field effect in self-assembled metallo-organic nanoscale networks

Mohammad S. Kabir, Andrey V. Danilov,[1] Leonid Y. Gorelik,[2] Robert I. Shekhter,[2] Mathias Brust,[3] and Sergey E. Kubatkin

Department of Microtechnology and Nanoscience (MC2), Chalmers University of Technology, S-41296, Göteborg, Sweden

[1]*also at Nano-Science Center (Department of Chemistry and Niels Bohr Institute), University of Copenhagen, Universitetsparken 5, DK-2100, Copenhagen, Denmark*

[2]*Department of Applied Physics, Chalmers University of Technology and Göteborg University, SE-412 96 Göteborg, Sweden*

[3]*Department of Chemistry, The University of Liverpool, Liverpool, L69 7ZD, United Kingdom*

Three-terminal devices have been produced by self-assembly of chemically stabilized gold clusters of 5–7 nm in diameter in a nanogap between the source and drain electrodes on top of an electrostatic gate made of oxidized aluminium. The conductivity of the devices with the agglomerates of clusters, self-assembled in the gap, was modulated substantially by the electric field of the gate. The effect is attributed to the mechanical deformation of the organic tunneling barriers between the gold clusters under the influence of Coulomb forces. A peculiar interplay between the mechanical deformations caused by the gate and the source-drain voltages leads to unusual current-voltage characteristics of the devices. A phenomenological theory based on these ideas has been developed.

PACS number(s): 85.85.+j, 81.16.Dn, 73.40.Gk

I. INTRODUCTION

Self-assembly of clusters helps to produce new materials with properties not previously observed in nature. Networks of chemically stabilized metallic clusters have electrical and optical properties that could be tuned through chemical control over cluster size and intercluster separation. Engineering of macroscopic properties by nanodesign offers many potentials for applications.

Tailoring the optical properties by nanodesign was demonstrated by Gotschy *et al.*[1] They studied the extinction spectra of regular arrays of metallic clusters fabricated by electron-beam lithography and demonstrated that the desired spectra can be achieved with a proper choice of cluster size and/or lattice parameter. Chumanov *et al.*[2] replaced lithographically defined structures with quasiregular two-dimensional arrays of silver clusters prepared by adsorption from colloidal suspensions. The extinction spectra were studied as a function of cluster-to-cluster distance which was varied by deposition density.

Even more promising is adjusting the material properties *in situ* by tuning the intercluster separation by mechanical deformation. Collier *et al.*[3] studied the optical response of monolayers of organically functionalized silver clusters and observed a dramatic effect of the surface pressure on the reflectance.

Not much experimental work exists regarding the study of electrical properties of self-assembled metallo-organic nanoscale networks. The bulk samples are poor conductors due to the hopping nature of intergrain electron transport,[4] though the dc conductance can be studied locally with scanning tunneling microscopy technique[5] or in a submicron gap between probe electrodes.[6–8] This activity was, in part, stimulated by a recent prediction of possible shuttle instability in these materials.[9]

Here we report the conductance measurements in a three-dimensional nanoscale network, self-assembled from chemically stabilized gold clusters in the nanogap between source and drain electrodes. The third electrode—the gate—was used to apply a static electric field. A giant field effect was observed, which we attribute to an exponential response of the tunneling conductance to the gate-induced mechanical sample distortion.

II. EXPERIMENT

A. Nanogap fabrication

A schematic picture of the device before cluster deposition is shown in Fig. 1(a). A planar gate electrode made of 250 Å aluminum covered by aluminum oxide was prepared on a chip of oxidized silicon. A shadow mask made by electron-beam lithography was used to deposit the 15-nm-thick gold lead electrodes on top of the gate, with an approximately 10-nm gap between the electrodes. We used a standard electrometric measurement scheme with a symmetric bias of the tunnelling gap; gate voltages of ±5 V could be applied without breakdown of the thin oxide layer on the gate [Fig. 1(a)].

B. Deposition of clusters

We used two different techniques to fabricate two different groups of self-assembled cluster devices. In the first group, the gold electrodes have been functionalized by dipping them in a neat 1,9 nonanedithiol. The clusters were then deposited using the following procedure: rinse in Hexane, dip in 1,9 nonanedithiol for 4.5 h, rinse in Hexane, dip in 6-nm thiol capped Au-cluster solution[10] for 26 h, rinse in Hexane. Clusters in these samples were linked to each other and to the gold electrodes, creating a 100-nm aggregate between the source and drain electrodes [atomic force microscope (AFM) image is in Fig. 1]. This assembly method relies on using a large excess of dithiol linker molecules, which ensures the spontaneous formation of a compact three-
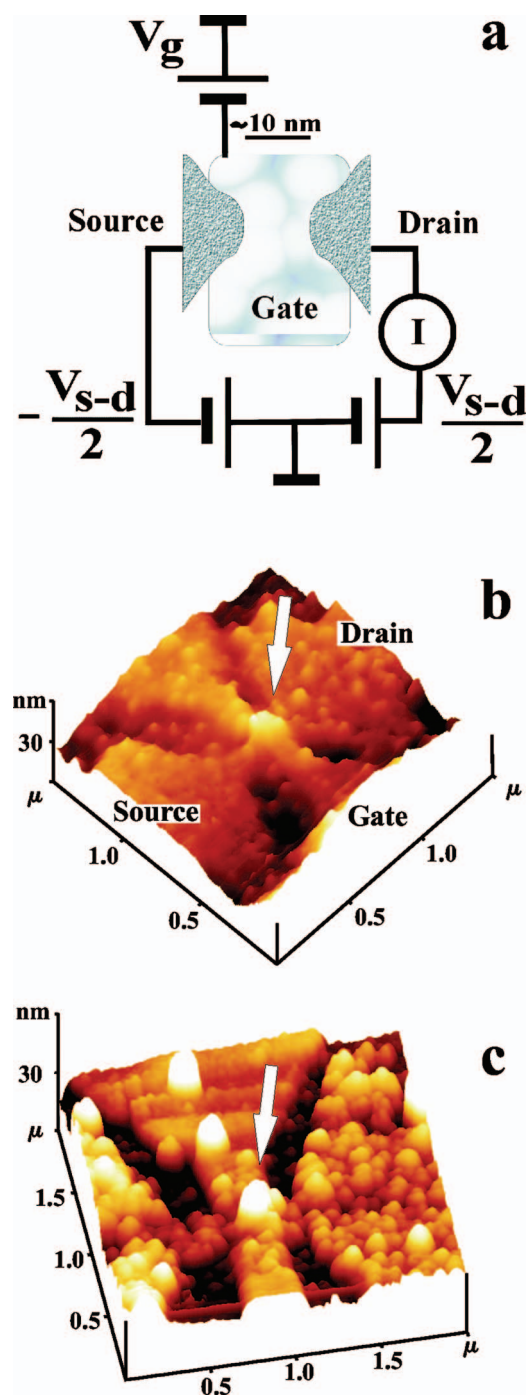
FIG. 1. (Color) (a) Three terminal measurement setup. (b) AFM image of the self-assembled $C_{12}H_{26}S$-capped Au clusters. The gold electrodes have been functionalized, so that the clusters are bonded to each other and to the gold electrodes. (c) Same as (b), but for the tetraoctylammonium-bromide-capped Au clusters. The gate oxide was functionalized, so that the clusters are bonded to the gate. Arrows on (b) and (c) point to humps of clusters of 100 nm between the source and drain electrodes.

dimensional network of dithiol cross-linked gold nanoparticles between source and drain electrode.

Samples of the second group have been prepared by functionalizing the aluminum oxide surface on top of an aluminum gate, so that the clusters were attached to the substrate.
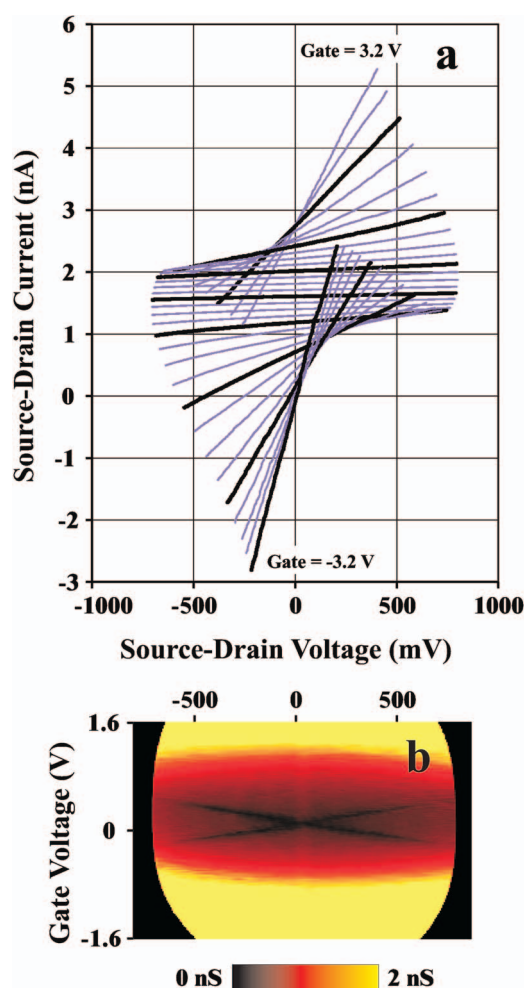

FIG. 2. (Color) Sample *A*. Clusters are bonded to the gold electrodes but not to the gate oxide. (a) A set of $I(V)$ curves taken at different gate voltages equally spaced in the range ±3.2 V. Curves are shifted for clarity. (b) Differential conductance dI/dV plotted in color scale in (V, V_G) plane. The contrast and tone curve are adjusted to highlight the crosslike structure formed by dI/dV minima.

The oxide layer was functionalized with 3-mercapto-triethoxypropylsilane by boiling for 15 min in 30 ml isopropanol containing ~ 0.03 ppm of silane, followed by thorough washing with isopropanol and curing in an oven for 5 min at 100 °C. The samples were then immersed in a solution of bromide stabilized gold nanoparticles[4] for 1–3 h. No thiol layer was applied to these samples. The rationale of this second assembly strategy was to achieve better control over the amount of nanoparticles assembled between the source and drain electrode. Ideally, the mercaptosilane forms a monomolecular layer on the gate oxide to which the gold nanoparticles would attach by binding to the terminal thiol groups of the silane molecules and thus form a two-dimensional assembly between the source and drain electrode. In reality, however, silanization always leads to the formation of some polymeric material bound to the treated surface, so that three-dimensional growth of the nanoparticle layer cannot be avoided in practice. For this reason, both groups of samples show some structural and electronic characteristics which have to be attributed to the presence of a
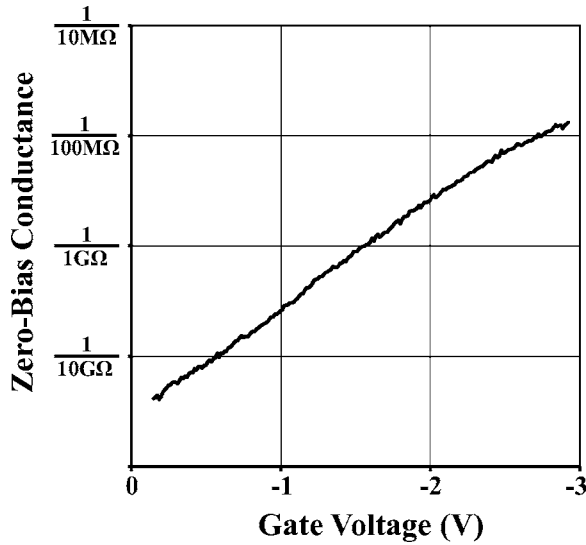
FIG. 3. Sample *A*. Zero-bias conductance $dI/dV|_{V=0}$ as a function of the gate voltage V_G. The conductance rises as $\exp(V_G/V_G^*)$, where $V_G^* \approx 0.43$ V.

three-dimensional network of particles and cannot be explained by the notion of a well-defined monoparticle layer on the substrate surface. In particular, the AFM images (Fig. 1) illustrate this situation. In both cases, what is imaged has to be interpreted as a three-dimensional aggregate of many particles between the source and drain electrode.

Below, we will present the data for two representative samples. Sample A is representative of the first group and the sample B of the second.[11]

C. Electrical measurements

All measurements have been performed at 4.2 K. Both samples demonstrated strong conductance modulation by the gate voltage. Properties of the sample *A* are summarized in Fig. 2. A series of current-voltage characteristics is shown in Fig. 2(a). The conductance has a minimum at low gate voltages, then rises significantly as the gate voltage increased, being an even function of the gate voltage. Zero-bias conductance of the sample is shown on a logarithmic scale in Fig. 3. We see that the plot is linear with gate voltage; this holds for a conductance variation of more than 100 times. We also observed a weak nonlinearity of the current-voltage characteristics—local depressions of the sample differential conductance, which were symmetric in source-drain voltage. This effect is shown in more detail in Fig. 2(b), where the color coded dI/dV is shown in the region of small gate voltages. The figure shows that the positions of the depressions in differential conductance form straight lines on the gate-bias plane.

The properties of the sample *B* are shown in Fig. 4. It also demonstrated strong modulation of the conductance by the gate voltage. Obviously, the nonlinearities of this sample are much more pronounced, as can also be seen from Fig. 4(b), where a set of dI/dV curves is shown for the range of gate voltages equally spaced between 0 and 5 V. At zero gate voltage, a single minimum of the differential conductance is

observed at zero source-drain voltage; this minimum is split into two when a certain threshold in the gate voltage is overcome. Beyond this threshold gate voltage, the zero-bias differential conductance is increasing. The color coded dI/dV pattern shows evolution of the peculiarities in differential conductance lines on the gate-bias plane. A wide dark line with a single dI/dV minimum is followed by *V*-shaped narrow dark lines corresponding to the splitted conductance minima at higher and/or lower gate voltages. Since we used a constant current measurement scheme, the voltage applied to the high conductive sample was limited; black areas in the plot of Fig. 4(c) correspond to the areas where data are missing.

III. DISCUSSION

A. General considerations

There are two important experimental observations: (i) The exponential dependence of the zero-bias conductance G as a function of the gate voltage V_G (Fig. 3)

$$G(V_G) \sim \exp(V_G/V_G^*). \tag{1}$$

(ii) The differential conductance dI/dV demonstrates splitting of the conductance minimum at some critical value of the gate voltage $\widetilde{V}_G$ (Fig. 4); this indicates that not only the gate voltage V_G, but also the source-drain voltage V affects the differential conductance. The general form describing the sample behavior in the vicinity of $\widetilde{V}_G$ is given by

$$\frac{dI}{dV}(V,V_G) = a - b(V_G - \widetilde{V}_G)V^2 + cV^4. \tag{2}$$

We shall see that both observations can be explained well by considering the mechanical deformations of cluster networks by Coulomb forces induced by the gate and source-drain voltages. Let us estimate the forces experienced by our cluster network at a typical voltage of 1 V applied to the gate. The first two to three layers of the gold grains screen the static gate potential, working together as a plate of a capacitor; mostly, these interface layers will be affected by the gate. With a gate oxide thickness of 5 nm, a metallic cluster of 5 nm in diameter will get an induced charge of as large as ten electrons and will be attracted toward the gate with the force of $\sim$3 nN. The curvature of the gold cluster concentrates this force on just a few molecules in the organic shell, producing a pressure of a few GPa. This pressure is strong enough to compress the shell noticeably, to change the intergrain distances, and to affect the tunneling barriers transparency. The described mechanism is the origin of the conductance modulation described in this paper.[12]

General electrostatics predict that Coulomb forces depend on a linear combination of V_G^2, V^2, and VV_G. While the first term is responsible for the exponential increase of the zero-bias conductance (1), the interplay between the latter two gives local dips in dI/dV.

Indeed, the term $\sim V^2$ arises because the bias voltage creates the potential gradient across the medium and, therefore, the grain-to-grain potential difference, which, in turn, leads
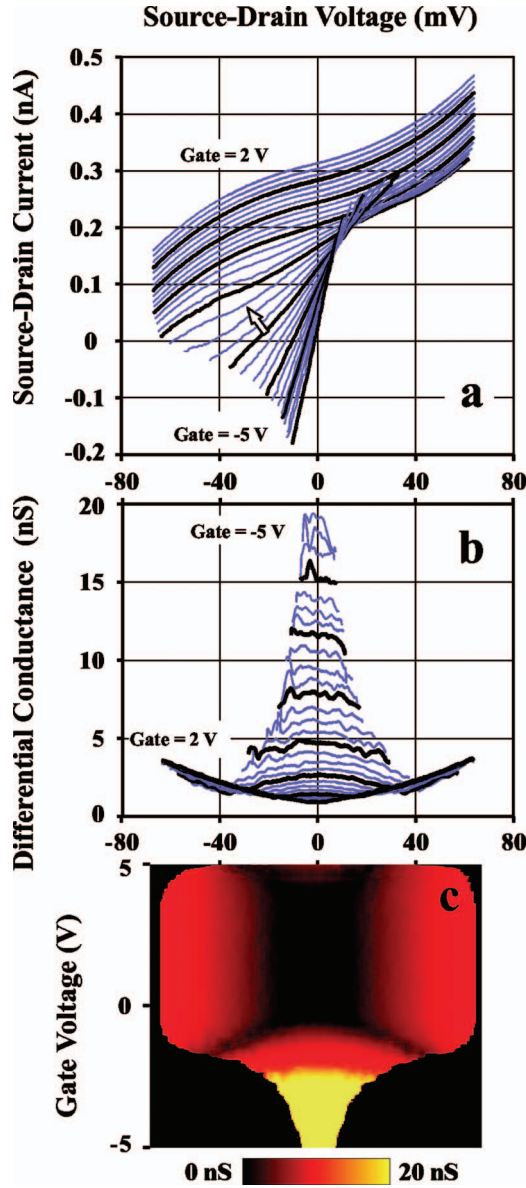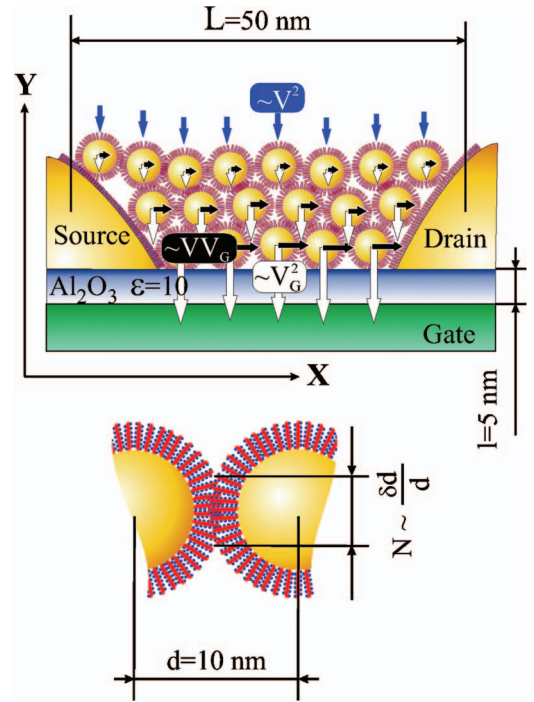
FIG. 5. (Color) (top) Three different groups of Coulomb forces. White arrows—(gate induced charge) $\times$ (gate voltage) $\sim V_G^2$. Black arrows—the lateral forces (gate induced charge) $\times$ (bias voltage) $\sim VV_G$. Blue arrows—the bias gradient leads to the mutual attraction between the gold grains, which is equivalent to a surface pressure $\sim V^2$. (bottom) The simplest model which leads to *stress* $\sim$ *strain*^{2} relation for the granular medium. The contact area (the number of stressed organic molecules N) is proportional to the strain $\delta d / d$. The gold clusters are nondeformable.

The mechanical properties of cluster networks are very peculiar. While most solids exhibit a linear strain-stress relation at low stresses, the elastic properties of granular materials follow a more general *stress* $\sim$ *strain*$^\eta$ law.[15] This nonlinearity has a clear physical nature: When the solid grains are pressed against each other, the contact area and, therefore, the number of organic molecules under stress increases and the granular medium become more rigid.

The exponent η of the stress-strain relation can be obtained from the zero-bias conductance plot in Fig. 3 assuming that the sample conductance depends exponentially on the strain caused by the electrostatic pressure $\sim V_G^2$. Since the conductance logarithm is a linear function of V_G in Fig. 3, we conclude that $\eta = 2$ (i. e. *stress* $\sim$ *strain*^{2}) in a wide range of gate voltages.[16]

B. Model description of the device

To develop a quantitative theory, we will treat the granular material as a uniform medium where the local conductivity exponentially depends on the local strain due to the tunneling nature of the charge transport. More specifically, we assume that the constant strain e_x along, say, the x direction results in a conductivity $G_{xx} = G_0 \exp(A_x e_x)$ where the constant A_x is about d_0 / λ ($d_0 \approx 10$ nm is grain-to-grain distance

FIG. 4. (Color) Sample *B*. Clusters are bonded to the gate oxide. (a) A set of $I(V)$ curves taken at different gate voltages equally spaced in the range -5–2 V. Curves are shifted for clarity. An arrow indicates a point on $I(V)$ curve where dI/dV has a minimum. (b) Differential conductance curves for the gate voltages equally spaced in the range 2–-5 V. Note that at $V_G = 0$ differential conductance has a single minimum at zero bias, while for $V_G < 0.5$ V, there exist two minima on dI/dV curve. (c) dI/dV plotted in color scale in (V, V_G) plane.

to the mutual attraction between the metallic grains. The term $\sim VV_G$ accounts for the fact that the bias-induced lateral electric field $E_x \sim V$ applied to a gate-induced surface charge $\sim V_G$ creates a sliding force $\sim VV_G$ (see Fig. 5). The lateral deformation always suppresses conductivity, and therefore, at high enough V_G, the differential conductance decreases with the bias voltage, i.e., $d^2 I/dV^2 < 0$. On the contrary, at high enough biases, the V^2 term always dominates VV_G and $d^2 I/dV^2 > 0$. Altogether, this leads to bifurcationlike behavior of the conductance (2).

and $\lambda \approx 1$ Å is characteristic tunnelling length of the —$(CH_2)_n$— molecular chain[17].

In the same way, the e_y strain increases $G_{yy} \exp(A_y e_y)$ times (for an isotropic material $A_x = A_y$). However, when the gate voltage increases the surface conductance by two orders of magnitude this symmetry is lifted, and we shall take the strain-conductance relation in a more general form

$$G_{ij} = G_0 e^{-\alpha e_{kk} + \beta [n_{ik} e_{kj} - n_{ij}(n_{kl} e_{lk})]}, \qquad (3)$$

where $n_{ij} \equiv n_i n_j$ and n_i is the vector normal to the gate surface. Note that α and β are of the same order of magnitude, because even when the material strain increases conductance 100-fold, G_{xx}/G_{yy} is still in the range 0.5–2.[18] Parameter α is positive (under pressure the medium is more conductive) while the sign of β is not defined.

Next, as discussed above, for small deformations, the irregular granular network is mechanically isotropic, with a stress tensor σ_{ij} *quadratic* in terms of strain tensor components e_{ij}

$$\sigma_{ij} = -K(e_{kk})^2 \delta_{ij} - 2\mu e_{kk}\left(e_{ij} - \frac{1}{3}e_{kk}\delta_{ij}\right) \qquad (4)$$

(where both K and μ are positive). This is the most general form, provided that the stress is zero for purely shear strain with $e_{ii}=0$. We can also note that for given material parameters d_0 and λ, the strain is only a few percent even for extreme conductance variations. Therefore, the form (4) is adequate even for strongest achievable deformations.[19]

To find the deformation, we shall solve static balance equations

$$\frac{\partial \sigma_{ik}}{\partial u_k} = -f_i \qquad (5)$$

with electrostatic forces $\vec{f} = \epsilon_0 (\nabla \vec{E})\vec{E}$ ($\vec{u}$ is a local medium displacement).

We assume that an electric field $\vec{E}$ has the gate-induced component $E_y \sim V_G$ and the bias-induced component $E_x \sim V$ (and $E_z = 0$). The y component is effectively screened within a thin surface layer Λ

$$E_y(y) = E_y \exp\{-y/\Lambda\} \qquad (6)$$

(see Fig. 5),[20] while the x component supports an electric current and, therefore, is not screened: $E_x(y) \equiv E_x$.

Eventually, the balance equations take the form

$$\frac{\epsilon_0}{\Lambda} E_x E_y e^{-y/\Lambda} = \frac{\partial}{\partial x}[(e_{xx} + e_{yy})(a e_{xx} - b e_{yy})]$$

$$+ \mu \frac{\partial}{\partial y}[(e_{xx} + e_{yy})e_{xy}],$$

$$-\frac{\epsilon_0}{\Lambda} E_y^2 e^{-2y/\Lambda} = \frac{\partial}{\partial y}[(e_{xx} + e_{yy})(a e_{yy} - b e_{xx})]$$

$$+ \mu \frac{\partial}{\partial x}[(e_{xx} + e_{yy})e_{xy}], \qquad (7)$$

where $a = (K + 4\mu/3)$ and $b = (K - 2\mu/3)$.

We shall solve (7) for the following boundary conditions: (a) $\sigma_{yy}(y=\infty) = \{[\varepsilon_0(1-\varepsilon)]/2\}E_x^2$; this accounts for the fact that a constant field E_x induces polarization, and therefore, mutual attraction of metallic grains. This is equivalent to a hydrostatic pressure $\sim E_x^2$ applied to a free sample surface.[21] The effective dielectric permittivity ϵ is defined by $\epsilon = 1 + 4\pi P/E$, where P is an average polarization in a volume much higher than d_0^3. (b) $\sigma_{xy}(y=\infty) = 0$; there are no bulk charges and, therefore, no shear forces far from the gate electrode. (c) $u_x(x = \pm L/2) = 0$; we take the simplest rectangular form for the source and/or drain electrodes. (d) $e_{yx}(y=0) = 0$; for the sample in Fig. 2, we assume that the granular medium is freely sliding against the gate electrode. Or, alternatively, (d′) $u_x(y=0) = 0$; for the sample in Fig. 4, we assume that for all grains in the first layer the lateral displacement is zero.

For zero-bias voltage ($E_x = 0$) Eqs. (7) have a trivial solution

$$e_{yy} = \sqrt{\frac{\epsilon_0}{2a}} E_y e^{-\frac{y}{\Lambda}}, \quad e_{xx} = e_{xy} = 0. \qquad (8)$$

We see that the strain is localized within a thin layer across the medium-gate interface. For all but the smallest gate voltages, the conductance of the surface Λ-layer defines the current. We also see that the zero-bias conductance changes as $\sim \exp(E_y/E^*)$, where the characteristic field $E^* = \sqrt{2a/(\epsilon_0 \alpha^2)}$.

For nonzero bias, we look for a solution of (7) in the form

$$e_{ij} = -\delta_{iy}\sqrt{\frac{\epsilon_0}{2a}[E_y^2 e^{-2y/\Lambda} + \varepsilon_0(\varepsilon-1)E_x^2]} + \tilde{e}_{ij},$$

where $\tilde{e}_{ij}$ satisfies the boundary conditions (b)–(d)/(d′) and also (ã) $\tilde{e}_{yi}(y=\infty) = o(e^{-y/\Lambda})$.

Finally, we note that $E_x/E_y \sim 10^{-3}$

$$E_y = \epsilon_{Al_2O_3} V_G/L \sim 1 \text{ V/nm} \gg E_x = V/L \sim 1 \text{ mV/nm}, \quad (9)$$

and we can linearize equations for $\tilde{e}_{ij}$ by disregarding the terms $O(E_x^3/E_y^3)$[22]

$$\frac{\partial}{\partial y}e^{-y/\Lambda}[2a\tilde{e}_{yy} + (b+a)\tilde{e}_{xx}] + \mu e^{-y/\Lambda}\frac{\partial}{\partial x}\tilde{e}_{xy} = 0,$$

$$e^{-y/\Lambda}\frac{\partial}{\partial x}[2b\tilde{e}_{yy} + (a+b)\tilde{e}_{xx}] + \mu \frac{\partial}{\partial y}e^{-y/\Lambda}\tilde{e}_{xy} = -\frac{2a}{\alpha\Lambda}\frac{E_x}{E^*}e^{-y/\Lambda}. \qquad (10)$$

The solution of (10) reads

$$\tilde{e}_{xx} + \tilde{e}_{yy} = \frac{a}{a+b}\frac{E_x}{E^*}\frac{x}{\Lambda}, \quad \tilde{e}_{xy} = 0, \qquad (11)$$

for the sample in Fig. 2 with the boundary condition (d) (no shear distortion for a free sliding sample) and

$$\widetilde{e}_{xx} + \widetilde{e}_{yy} = 0, \quad \widetilde{e}_{xy} = \frac{2a}{\alpha\mu}\frac{E_x}{E^*}, \tag{12}$$

for the sample in Fig. 4 with the boundary condition (d') (shear distortion with zero dilatation).[23]

Taking into account the fact that the current goes through a thin layer with a thickness $\Lambda < L$ (i.e., that the y component of the current density is negligible), we have for an $I(V)$

$$I = \frac{V}{L^{-1}\int_{-L/2}^{L/2} dx \left(L_z \int_0^\infty dy \rho_{xx}^{-1} \right)^{-1}}, \tag{13}$$

where $\rho_{xx} \equiv (g_{ij}^{-1})_{xx}$ and L_z is the effective thickness of the conducting layer in the z direction. After integration, we arrive at

$$I = G(V_G)Ve^{\eta\frac{V^2}{V_G V_G^*}} \begin{cases} \eta_s \dfrac{l}{\Lambda}\dfrac{V}{V_G^*}\sinh^{-1}\left(\eta_s \dfrac{l}{\Lambda}\dfrac{V}{V_G^*}\right) & \text{(sliding sample in Fig. 2)} \\[2ex] \cosh^{-1}\left(\eta_g \dfrac{V}{V_G^*}\right) & \text{(nonsliding sample in Fig. 4)} \end{cases}, \tag{14}$$

where $G(V_G)$ is zero-bias conductance for the gate V_G, $V_G^* = E^* l / \epsilon_{Al_2O_3}$, $\eta = \{[\epsilon^2(\epsilon-1)]/\epsilon_{Al_2O_3}^2\}(l^2/L^2)$, $\eta_g = (\beta/\alpha)(\epsilon/\epsilon_{Al_2O_3})(l/L)$ and $\eta_s = \{a/[2(a+b)]\}(\epsilon/\epsilon_{Al_2O_3})$.

From (14) one can see that zero-bias curvature of $I(V)$ curve, d^2I/dV^2, is positive for $V_G=0$ and changes sign at

$$\widetilde{V}_G = V_G^* \begin{cases} 6(\eta/\eta_g^2)(\Lambda/L)^2 & \text{(sample in Fig. 2)} \\ 2(\eta/\eta_g^2) & \text{(sample in Fig. 4)} \end{cases}. \tag{15}$$

We note that the result does not depend on the sign of the parameter β and $\eta/\eta_g^2 = (\alpha/\beta)^2(\epsilon-1)$, where $\alpha/\beta \sim 1$ [see discussion after formula (3)]. To estimate the effective ϵ for the granular medium, we take $(\epsilon-1) \approx (\epsilon_{org}-1)v \approx 1$, where for self-assembled organic monolayer $\epsilon_{org} \approx 3$,[24] and $v \approx 0.5$ is the volume fraction occupied by the organic molecules (note that the volume fraction occupied by the gold grains is negligible).

For a sample bound to the substrate the second formula in (15), therefore, gives $\widetilde{V}_G \sim V_G^*$, i.e., the conductance minimum splits into two minima approximately when the zero-bias conductance increases e times, in a good agreement with experimental data.[25] This is a very general result, which does not depend on the phenomenological parameter Λ and is insensitive to the not-so-well-defined sample dimensions.

To estimate V_G^*, we shall evaluate the material parameter a for the granular medium in (8). We take the next approximation and consider the organic interlayer as an array of *independent* springs each following the Hook's law. While the elastic force from each spring is proportional to the dilatation $\Theta = e_{ii}$, the number of springs within the contact area also increases as Θ, so that the total force scales as Θ^2. A simple integration shows that

$$\sigma = \frac{\pi d_0}{2L_{mol}}K_{org}\Theta^2, \tag{16}$$

which defines K in (4) in terms of the Young's modulus K_{org} for the uniform organic medium ($L_{mol}=1.4$ nm is the length of the $C_{12}H_{26}S$ molecule). Taking $K_{org}=3-5$ GPa (a typical

value for organic materials[28]) and assuming that μ is the same order of magnitude as K, we arrive at $V_G^*=0.4-0.6$ V, which is in a good agreement with experimental data 0.43 V (Fig. 3).

For a free sliding sample, the first formula in (15) gives $\widetilde{V}_G \ll V_G^*$. For such small gate voltages, the condition that the current mainly goes through a thin layer on top of the gate electrode is not valid, i.e., the main assumption for (10)–(13) does not hold. However, the result (15) ensures that for gate voltages down to at least $\sim V_G^*$ the dI/dV has two minima.

To analyze what happens at lower gate voltages, we go back to the balance equation (7) and note that it has a remarkable scaling symmetry: When both E_x and E_y are scaled k times, the deformation field e_{ij} also scales k times, i.e., $e_{ij}(kV, kV_G) = ke_{ij}(V, V_G)$. On the other hand, for $V_G < V^*$ the deformation e_{ij} is so small that (3) reduces to[32] $G_{ij} \approx G_0\delta_{ij}(1-\alpha e_{ii})$, and we can write

$$G_{ij}(kV, kV_G) = G_0\delta_{ij} + G'_{ij}(kV, kV_G) = G_0\delta_{ij} + kG'_{ij}(V, V_G), \tag{17}$$

where G' is the field-induced correction to the main conductance G_0. As this correction is small, (18) is equivalent to a scaling formula for the total current

$$I(kV, kV_G) = kV/R + I'(kV, kV_G) = kV/R + k^2 I'(V, V_G), \tag{18}$$

where I' is nonlinear part of $I(V)$ curve and R is the sample resistance at zero bias. An immediate consequence of (18) is $(\partial^2 I/\partial V^2)(kV, kV_G) = (\partial^2 I/\partial V^2)(V, V_G)$, and we see that if $\partial I/\partial V$ has minima at some (V, V_G) point, it also has a minima at (kV, kV_G), i.e., on the V-V_G plane, the minima shall be positioned along the straight lines crossing at (0, 0) point, exactly as in Fig. 2(b).

To conclude, the difference in transport properties of the two types of samples is due to the different strengths of lateral deformation. The deformation is much stronger for the samples with thiol-stabilized clusters, which are free to

slide against the substrate. As a result, $d^2I/dV^2(0, V_G) < 0$ for all the gate voltages. In contrast, in the samples with bromine-stabilized clusters (linked to the substrate), the lateral displacement starts to dominate over the bulk compression only at some critical gate voltage.

IV. CONCLUSION

In summary, we have demonstrated a significant conductance modulation in self-assembled nanoscale networks of metallic clusters bridged by organic molecules. We argue that the observed effects have nanoelectromechanical origin and a theoretical model that can account for the most important experimental observations is presented. The conductance modulation based on the variation of the tunneling barrier width promises successful device operation at room temperatures. This self-assembled multicluster nanodevice is more tolerant to variations in cluster position than the single electron transistor geometry, where a single cluster must be put in the tunneling gap and, therefore, promises wider fabrication margins and higher yield in production.

[1] K. Gotschy, K. Vonmetz, A. Leitner, and F. R. Aussenegg, Appl. Phys. B **63**, 381 (1996).

[2] G. Chumanov, K. Sokolov, and M. T. Cotton, J. Phys. Chem. **100**, 5166 (1996).

[3] C. P. Collier, R. J. Saykally, J. J. Shiang, S. E. Henrichs, and J. R. Heath, Science **277**, 1978 (1997).

[4] M. Brust, D. Bethel, C. J. Kiely, and D. J. Schiffrin, Langmuir **14**, 5425 (1998).

[5] D. I. Gittins, D. Bethell, D. J. Schiffrin, and J. Nichols, Nature (London) **408**, 67 (2000).

[6] R. P. Andres, J. D. Bielefeld, J. I. Henderson, D. B. Janes, V. R. Kolagunta, C. P. Kubiak, W. J. Mahoney and R. G. Osifchin, Science **273**, 1690 (1996).

[7] S. H. M. Persson, L. Olofsson, and L. Gunnarson, Appl. Phys. Lett. **74**, 2546 (1999).

[8] T. Hassenkam, K. Moth-Poulsen, N. Stuhr-Hansen, K. Nørgaard, M. S. Kabir, and T. Bjørholm, Nano Lett. **4**, 19 (2004).

[9] L. Y. Gorelik, A. Isacsson, M. V. Voinova, B. Kasemo, R. I. Shekhter, and M. Jonson, Phys. Rev. Lett. **80**, 4526 (1998).

[10] M. Brust, M. Walker, D. Bethell, D. J. Schiffrin, and R. Whyman, J. Chem. Soc., Chem. Commun. **7**, 801 (1994).

[11] As can be seen from AFM image, despite the difference in fabrication, the sample B is topographically very similar to the sample A: in both samples, there is a hump of clusters of 100 nm between the electrodes. It is unclear why clusters are concentrated between the electrodes in both fabrication recipes; possibly a surface tension keeps the last drying droplet of solvent between the electrodes, thus concentrating clusters and producing a hump.

[12] Compare to mechanical stress effects in thick-film resistors (Refs. 13 and 14).

[13] G. E. Pike, and C. H. Seager, J. Appl. Phys. **48**, 5152 (1977).

[14] C. Canali, D. Malavasi, B. Morten, M. Prudenziati, and A. Taroni, J. Appl. Phys. **51**, 3282 (1980).

[15] A. T. Skjeltorp and S. F. Edwards, *Soft Condensed Matter: Configurations, Dynamics and Functionality*, Series C: Vol. 552 (Kluwer, Dordrecht, 2000) p. 5.

[16] The exact value of η is not important, however. The simple model description presented in Sec. III B holds for all $\eta > 1$.

[17] L. A. Bumm, J. J. Arnold, T. D. Dunbar, D. L. Allara, and P. S. Weiss, J. Phys. Chem. B **103**, 8122 (1999).

[18] This can be directly shown for some regular (triangular, honeycomb) lattices.

[19] The reason why we can use *isotropic* form (4) for mechanical properties, while we must use the *nonisotropic* form (3) for a conductance is that a *small* stress $e \sim 10^{-2} \ll 1$ causes the *strong* conductance change $\sim 100 \gg 1$.

[20] This continuum model is formally valid if only Λ is much higher than d_0. In fact, Λ/d_0 is only about $\sim$2–3. However, as we shall see below, the model still adequately reproduces all essential experimental findings.

[21] L. D. Landau, E. M. Lifshitz, and L. P. Pitaevskii, *Electrodynamics of Continuous Media*, 2nd ed. (Butterworth-Heinemann, Oxford, U.K., 1998) Sec. 15, p. 62.

[22] Note that while the gate voltage changes conductance 100 times, the $\sim VV_G$ and $\sim V^2$ terms cause only moderate ($\sim$25%) nonlinearity of differential conductance. I.e., the bias-induced effects are indeed small corrections to the leading effect of the gate voltage.

[23] Formally, solutions (11) and (12) do not satisfy the boundary conditions at $x = \pm (L/2)$. But as soon as $\Lambda/L < 1$, we can disregard small edge effects.

[24] M. A. Rampi, O. J. A. Schueller, and G. M. Whitesides, Appl. Phys. Lett. **72**, 1781 (1998).

[25] Some asymmetry between positive and negative gates in Fig. 4 is due to the intrinsic polarization of the self-assembled monolayer, which was used to functionalize the gate oxide (see Refs. 26 and 27) for sample B.

[26] J. Takeya, T. Nishikawa, T. Takenobu, S. Kobayashi, and Y. Iwasa, Appl. Phys. Lett. **85**, 5078 (2004).

[27] K. P. Pernstich, S. Haas, D. Oberhoff, C. Goldmann, D. J. Gundlach, B. Batlogg, A. N. Rashid, and G. Schitter, J. Appl. Phys. **96**, 6431 (2004).

[28] The -(CH$_2$)- molecular chain itself is rather rigid. The predicted value for the Young's modulus in a perfect monolayer is about 80 GPa (see Ref. 29). Close value was observed in experiments with near perfect alkane monolayers sandwiched between planar metallic surfaces (see Ref. 30). However, the presence of the defects in the organic bridges decreases the Young's modulus down to a few GPa (see Ref. 31).

[29] A. B. Tutein, S. J. Stuart, and J. A. Harrison, J. Phys. Chem. B **103**, 11357 (1999).

[30] C. N. Lau, D. R. Stewart, R. S. Williams, and M. Bockrath, Nano Lett. **4**, 569 (2004).

[31] D. L. Patrick, J. F. Flanagan, P. Kohl, and R. M. Lynden-Bell, J. Am. Chem. Soc. **125**, 6762 (2003).

[32] We also put $\beta=0$ because for small distortions the medium is isotropic.